CHEMISTRY

Long-range, selective, on-demand suspension interactions: Combining and triggering soluto-inertial beacons

Anirudha Banerjee and Todd M. Squires*

Structures and particles that slowly release solute into solution can attract or repel other particles in suspension via diffusiophoresis, a process we termed "soluto-inertial (SI) interactions." These SI interactions involve "beacons" that establish and sustain nonequilibrium solute fluxes over long durations. Here, we demonstrate the versatility of the SI concept and introduce distinct strategies to manipulate solute gradients and, hence, suspension behavior using beacons with different physicochemical properties. First, we demonstrate on-demand particle migration using beacons that can be actuated with a trigger. We then show the synergy between multiple, distinct beacons that modify solute fluxes in a way that allows directed, yet selective, colloidal migration to specific target sites. Moreover, this multibeacon harmony enhances migration velocities, and delays the equilibration of the SI effect. The different SI techniques highlighted here suggest previously unidentified possibilities for sorting and separating colloidal mixtures, targeting particle delivery, and enhancing rates of suspension flocculation.

INTRODUCTION

Complex fluids are all around us—in commercial products such as lubricants (*1*), paints (*2*), and cosmetics (*3*); in physiological (*4*), biological (*5*), and naturally occurring systems (*6*); in industrial processes (*7*); in foodstuffs (*8*); and in emerging technologies (*9, 10*). Common to these diverse systems are colloidal-scale macromolecular constituents. The design, formulation, and performance of soft materials depend critically on the interactions between these colloidal particles and their response to externally applied forces and fields (*11*).

Our ability to predict and control colloidal interaction and response underpins the ubiquity of soft materials. However, equilibrium interactions between colloids—including van der Waals, electrostatic, steric, and depletion forces—are typically restricted to distances ≤ 1 μm, thereby limiting the range over which interactions can be tuned (*12*). This length scale can be increased by applying external fields to drive colloidal systems out of equilibrium in a controlled manner (*13*), e.g., using optical (*14*), electric (*15*), and magnetic fields (*16*); shear flow (*17*); confinement (*18*); and interfacial curvature (*19*).

Subtler are gradients in solute concentration (or, equivalently, chemical potential) that can also extend the range of colloidal interactions. Migration of colloids under such gradients is known as diffusiophoresis (DP), where the magnitude and direction of particle motion are governed by the specific solute–particle surface interaction (*20*–*23*). DP is responsible for various nonequilibrium fluxes driving colloidal migration, including dissolving salt (*24*) and gasses (*25*), ion exchange membranes (*26*), transport into and out of dead-end pores (*27*, *28*), membrane fouling (*29*), and latex deposition (*20*). We recently established the concept of soluto-inertial (SI) interactions, which involve SI "beacons" that slowly release solute, driving particles to migrate via DP either up or down the solute flux (i.e., toward or away from the beacon), depending on the solute–particle surface interaction (*30*). The term "soluto-inertia" was chosen by analogy with thermal inertia, wherein high–heat capacity objects in poor heat-transfer media respond very slowly to changes in environmental temperature and, therefore, maintain heat flux over extended periods of time. These SI interactions require three ingredients (Fig. 1A): (i) an SI beacon with a high solute capacity (analogous to high thermal inertia of materials) responsible for establishing and maintaining solute flux over sustained periods of time, (ii) a solute that mediates the interaction, and (iii) colloidal particles that respond to the flux and migrate via DP.

Here, we highlight the versatility of the SI concept, demonstrating suspension interactions mediated by beacons with a variety of qualitatively distinct physicochemical properties. Figure 1 depicts the new SI strategies explored here. In particular, we first describe a class of thermoresponsive beacons that can be actuated with temperature as a trigger to release trapped solute and initiate DP migration in neighboring particles (Fig. 1, B-1 and B-2). Next, we combine distinct beacons and introduce SI dipole interactions where a beacon "source" releases solute, which is absorbed by a beacon "sink." This dipolar flux directs particle motion to propagate along well-defined trajectories, as depicted in Fig. 1C. Alternatively, multiple beacon sources, each emitting a different solute, provide new mechanisms to separate colloidal mixtures (Fig. 1D). A final variant on the multisource beacon strategy involves SI beacons that release solutes that react with each other (Fig. 1E). We show that this reaction results in faster, longer-lasting SI migration and enables targeting colloids to "focus" at intermediate locations in the suspension. We anticipate that this suite of conceptually new SI techniques and capabilities will find application in targeted particle delivery, enhancing the rate of particle aggregation in dilute suspensions that is otherwise limited by Smoluchowski's diffusion limitation (*31*), and as a new route toward advanced particle separations.

RESULTS

Triggered solute release and SI migration

The SI concept refers to beacons that absorb or release large amounts of solute in response to change in background solute concentration. Typically, SI beacons respond immediately when placed in contact with a solution with mismatched solute concentration below the equilibrium value. Here, we demonstrate advanced strategies that use an external trigger to initiate SI outflux from the beacon.

Department of Chemical Engineering, University of California, Santa Barbara, Santa Barbara, CA 93106-5080, USA.
*Corresponding author. Email: squires@engineering.ucsb.edu

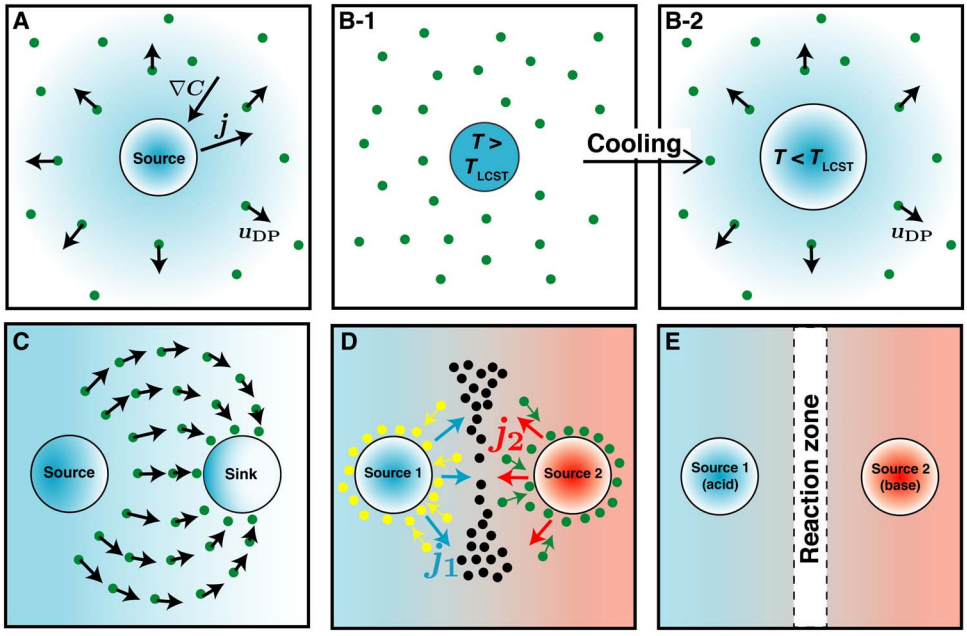

Fig. 1. Using SI beacons of one or more types to drive controlled colloidal migration. (**A**) A single SI beacon source that maintains solute outflux, driving DP migration (here down gradient) of particles, giving SI "repulsion." (**B-1**) Triggered release: A thermosensitive beacon keeps solute trapped at high-enough temperature ($T > T_{LCST}$); (**B-2**) upon cooling below LCST, the beacon releases the solute, initiating SI migration. (**C**) SI dipole: SI beacon source emits solute, as in (A), whereas the SI beacon sink absorbs the solute, establishing an SI dipolar flux that directs particle migration from one beacon to the other. (**D**) Combining SI beacon sources releasing distinct solutes may attract one particle species (yellow) to one source, a second species (green) to a second source, and repelling a third species of particle (black) from both. (**E**) SI beacon sources releasing solutes that react with one another (e.g., acid-base) establish long-lasting fluxes from each beacon to the reaction zone, driving particles accordingly.

We use the temperature-sensitive polymer poly-*N*-isopropylacrylamide (pNIPAm) cross-linked with methylenebisacrylamide to make hydrogels (SI beacons) (*32*) using the projection lithography technique described previously (*30*). pNIPAm has a lower critical solution temperature (LCST) of about 33°C (*33*). At temperatures below this LCST, it swells and absorbs water, whereas above the LCST, it phase separates into a dense polymer phase that expels solvent. We exploit this feature to trap solute within the beacon above the LCST. When it is cooled below the LCST, however, the hydrogel beacon swells, opening its pores and releasing the trapped solute.

Figure 2A shows a pNIPAm beacon at 50°C, above the LCST, so that the pNIPAm forms a dense, collapsed polymer phase that traps the residual photoinitiator (α-ketoglutaric acid), which will serve as the SI solute. Negatively charged polystyrene (PS) particles are expected to electro-diffusiophoretically move down acidic gradients (*34*), and we confirm this trend for α-ketoglutaric acid using the three-channel microfluidic DP device of Paustian *et al.* (*35*) in fig. S1. As long as $T >$ LCST, particles show no sign of DP migration, which would imply solute release (movie S1 and first 300 s of the blue data points in Fig. 2E). Upon cooling below LCST, the pNIPAm beacon expands (red dashed circle, Fig. 2B), releasing solute that drives SI repulsion of particles well beyond the edge of the swelling beacon (Fig. 2B and blue data points in Fig. 2E). As control, Fig. 2C and movie S2 show a pNIPAm hydrogel from which all solute has been flushed and then raised above LCST. As the beacon is cooled below LCST, it swells as in Fig. 2B. In this case however, no solute is released that would drive SI DP, and so particles simply move to accommodate the expanding gel (Fig. 2D and red data points in Fig. 2E). The particle interface coincides with the beacon boundary, which quickly reaches a new radius upon cooling.

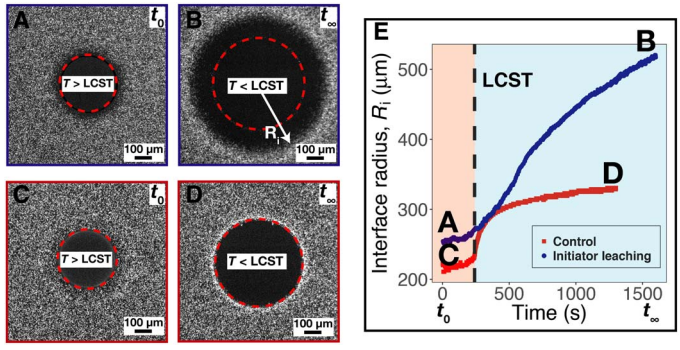

Fig. 2. Triggered solute release and SI migration using pNIPAm beacons. (**A**) A pNIPAm gel above the LCST can be used to trap solute molecules. The dashed red line shows the gel boundary. (**B**) The gel swells when it cools below the LCST, and the trapped solute diffuses out, establishing a concentration gradient that causes neighboring particles to migrate via DP. Control experiment: (**C**) The gel above the LCST closes its pores and occupies a smaller volume. (**D**) As the gel cools down, the pores open up and it expands, pushing the neighboring particles out of the way. (**E**) Points represent the change in the particle interface radius (R_i) as the gels undergo transition at the LCST.

Source-sink pairs of SI beacons: SI dipole

The next strategy involves sculpting solute fluxes using one beacon as source to emit solute [here sodium dodecyl sulfate (SDS)] and a second (empty) beacon as sink to absorb it. SI migration of particles is directed from the source to the sink as the diffusive solute flux forms a dipole. This targeted delivery of suspended particles represents enhanced control over DP migration compared with the single-source case.

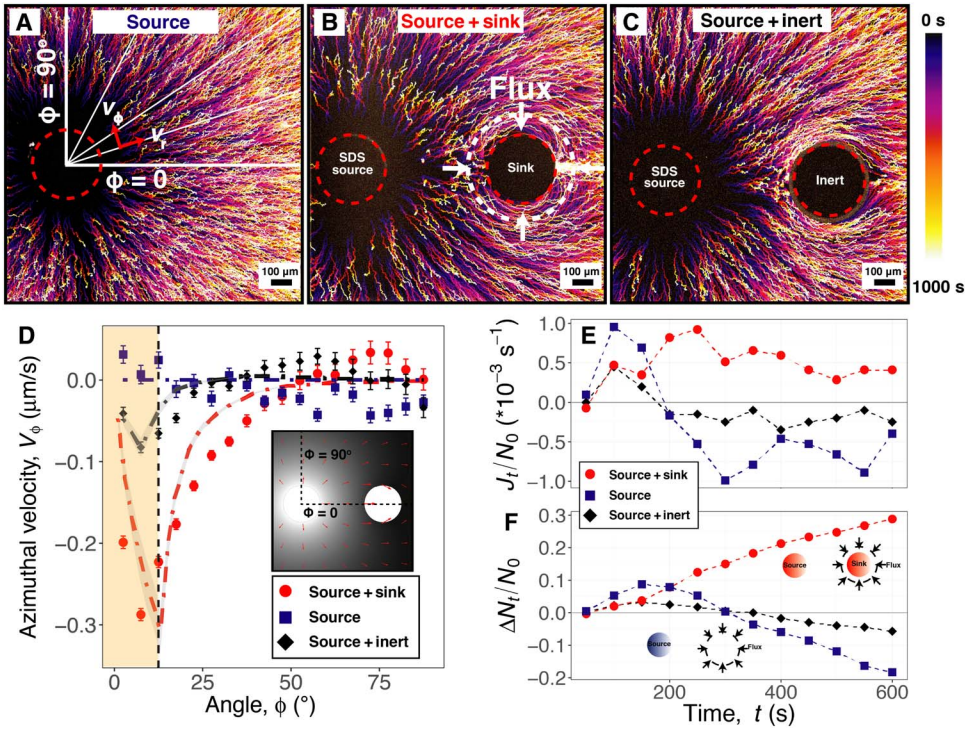

Fig. 3. SI source-sink dipole. Streak lines showing the trajectories of negatively charged PS particles migrating due to (**A**) an SDS source, (**B**) both SDS source and sink, and (**C**) an SDS source and an inert obstacle that does not absorb SDS. (**D**) Time-averaged azimuthal particle velocities as a function of angular position with respect to the source center under the scenarios depicted in (A) to (C). Error bars represent SD. Points show experimental data. Lines are predictions from COMSOL computations. Details of the COMSOL model are provided in the Supplementary Materials. The shaded region shows angle subtended by sink at source center, $\phi_{sink} = 12.5°$. The inset shows the solute concentration field and local particle velocities as computed by COMSOL. (**E**) Flux of particles, J_t, entering a region with radius $r = 1.5*R_{beacon}$ around the sink. (**F**) Cumulative particles captured in the region as function of time (as a fraction of number of particles in that region at $t = 0$, N_0). Dashed lines are for visual guidance.

Moreover, as DP velocities, u_{DP}, typically scale as the inverse of the solute concentration [$u_{DP} \propto \nabla \ln C$ (*21*, *22*)], SI dipoles can enhance u_{DP} and increase the duration of particle migration by maintaining a low background concentration, compared with an isolated source.

Figure 3A shows an isolated SI source releasing SDS, which drives radial migration of negatively charged PS particles, away from the beacon, consistent with previous findings (*30*, *36*). The solute gradient and, hence, the particle motion are notably altered when a sink absorbs SDS, causing colloids to be directed into the sink (Fig. 3B and movie S3). A third, control experiment (Fig. 3C) is also performed using an inert obstacle in place of the solute sink to show that solute absorption is responsible for the dipolar DP pattern, not merely the physical presence of a second beacon.

While the streak lines shown in Fig. 3 (A to C) display qualitative features of SI migration behavior, particle tracking reveals quantitative details. For example, the azimuthal particle velocity, V_ϕ, is approximately zero around the isolated SI source (blue squares in Fig. 3D), as expected for radial migration. Similarly, $V_\phi \approx 0$ for radial SI repulsion for the source and inert obstacle case (black diamonds), except near the obstacle. For the source-sink dipole however, $V_\phi \neq 0$ (red circles). This source-sink SI migration behavior is confirmed using numerical computations on COMSOL, by first computing the diffusive flux between the source and the sink and then calculating $u_{DP} \propto \nabla \ln C$ (dashed lines in Fig. 3D; see the Supplementary Materials, movie S4).

Figure 3E shows the flux of particles "collected" by the sink, determined by counting the change in the number of particles inside a circular region of radius $r = 1.5*R_{beacon}$ around the sink per unit time, $J_t = \frac{1}{\Delta t}\sum_t^{t+\Delta t} N_{in} - N_{out}$. This flux is normalized by the total particles in that region counted at time $t = 0$, N_0. For both the isolated source (Fig. 3E, blue squares) and inert obstacle (black diamonds), this flux is initially positive as particles are repelled from the source, and a repulsion "front" enters the region, and then becomes negative after approximately 200 s once the repulsion front passes beyond the region of interest. The source-sink pair, by contrast, shows particle collection persisting for at least 600 s (red circles). The cumulative change in particle collection, $\Delta N_t = \sum_0^t N_{in} - N_{out}$ (normalized by N_0), shown in Fig. 3F, increases monotonically for the dipole, yet becomes negative after about 300 s for the other two cases, indicating a net loss of particles.

Pairs of SI beacon sources loaded with distinct solutes

Multiple SI beacon sources, each emitting a distinct solute, may be combined to enable more complex particle collection strategies. For example, one source may repel particles, while the other may attract, similar to the source-sink case, although with distinct solutes. The two beacons create a composite solute gradient, which hastens migration from one to the other. This is shown in Fig. 4A (and movie S5), where an SDS source (blue circle) repels negatively charged PS particles while a second beacon emitting the ionic liquid 1-hexyl-3-methylimidazolium iodide ([C_6mim][I]; red circle) attracts particles. The combined effect is particle migration toward the right-hand beacon. The streak lines show particle trajectories over the first 1000 s of the experiment.

To quantify the enhancement of both the magnitude and duration of u_{DP}, we calculate the average velocity of particles in the region between the two beacons as a function of time (Fig. 4B). We compare the speed

and duration of migration under the composite solute gradient with those measured under each of the single solute gradients. Our observations are as predicted: The composite gradient (black points) results in faster particle migration in the interbeacon region compared with either of the two single solute gradients (blue diamonds and red circles). However, the resultant velocity under the composite gradient is less than the simple superposition of contributions from the individual sources (purple dashed line), as discussed later.

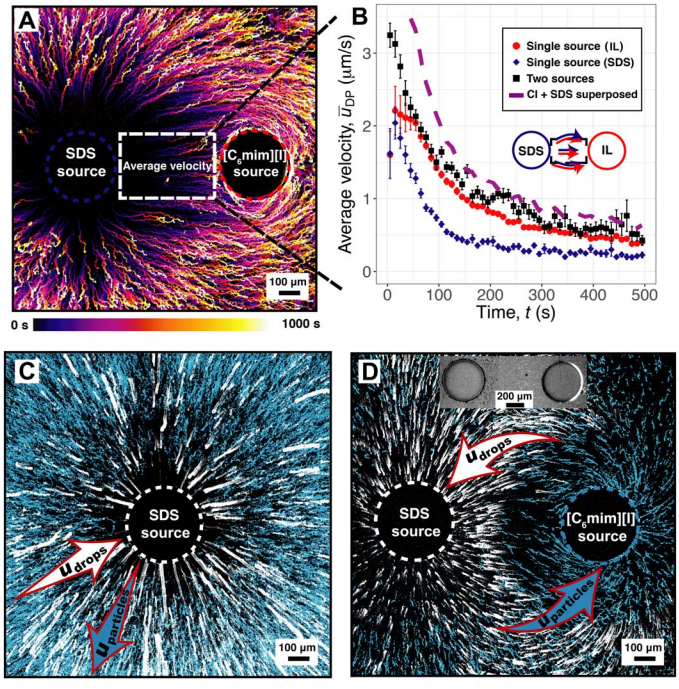

Fig. 4. SI migration driven by two sources releasing distinct solutes. (**A**) Streak lines show negatively charged PS particles repelled by SDS source and attracted to ionic liquid (IL), [C_6mim][I] source. (**B**) SI particle velocities, averaged in the interbeacon region, are larger when migrating under the composite gradient (black squares), compared with under either source in isolation, although slower than simple superposition of the two sources (purple dash). Error bars show SD. (**C**) An SDS source repels negative PS particles (blue streaks) but simultaneously attracts decane drops (white streaks). (**D**) Distinct beacon sources, one releasing SDS (left) and the other releasing IL, [C_6mim][I] (right). Decane drops (white) migrate toward the SDS source beacon, whereas negative PS beads migrate toward the [C_6mim][I] source beacon. Inset shows accumulation of decane (black) and PS (white) particles around the two beacons at the end of the experiment.

The direction of particle migration depends on the nature of interaction between the solute and the particle surface. We had previously exploited this feature to demonstrate oppositely directed migration of negative PS beads and decane drops under an SDS gradient generated by a single beacon source (Fig. 4C and movie S6) (*30*). Here, we use the same principle to show that a combination of beacon sources releasing distinct solutes (SDS and [C_6mim][I] in this case) causes negative PS beads to be attracted by the [C_6mim][I] source (blue streaks in Fig. 4D and movie S7), and decane drops by the SDS source (white streaks). The particles are eventually separated from the mixture, as seen in the inset of Fig. 4D—dark decane drops collect around the SDS beacon, while a bright PS cloud forms around the [C_6mim][I] beacon. The attraction of decane drops by an SDS source is not explained by DP but is rather a consequence of soluto-capillary migration and is discussed later.

Pairs of SI beacon sources loaded with reactive solutes

Last, we show that SI migration can be driven by two (or more) solute species that react with one another at an intermediate location. A strong flux of each reactant is directed to the reaction zone in this case, as the reactants are constantly consumed in the reaction. For example, a reactive multisource system is shown in Fig. 5, where the reaction between $Ca(OH)_2$ (calcium hydroxide) and $C_7H_6O_2$ (benzoic acid) drives positively charged PS particles toward the acidic beacon (Fig. 5A and movie S8) and negatively charged PS particles toward the basic beacon (Fig. 5B and movie S9). The streak lines show particle trajectories over the first 1000 s of the experiment.

In addition to maintaining long-lived solute fluxes, reactive solutes prevent background solute concentration from growing continuously, which would generally suppress u_{DP}, since it is proportional to $\nabla \ln C$. Figure 5C shows the average particle velocities in the interbeacon region as a function of time for the acid-base reaction (black diamonds), and under the single-component gradients of benzoic acid (blue squares) and calcium hydroxide (red circles). In the reactive, two-solute system, a steady particle flux is sustained for thousands of seconds with higher migration velocities, compared with SI migration under the individual sources.

Thus far, SI beacons have been charged with solute by exploiting associative interaction between polymer and solute (*37*, *38*). In this case however, we precipitate the solutes $Ca(OH)_2$ and $C_7H_6O_2$ inside the

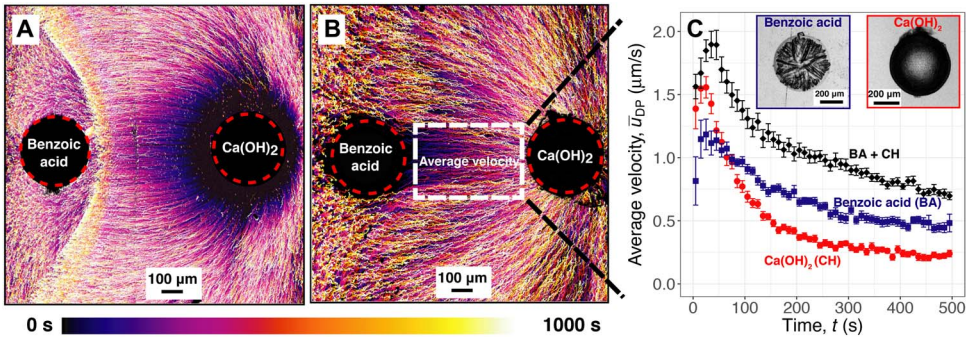

Fig. 5. SI migration driven by reactive solutes. Streak lines showing migration under the flux generated by the reaction between $Ca(OH)_2$ and benzoic acid. (**A**) Aminated (positive) PS particles migrate toward the acidic beacon, while (**B**) sulfonated (negative) PS particles migrate toward the basic $Ca(OH)_2$ source. (**C**) Beads migrate the fastest and for a longer duration when there is a reaction between the acid and the base (black diamonds) as opposed to migrating under the flux of acid (blue squares) or base (red circles) alone. Error bars show SD. Inset shows $Ca(OH)_2$ and $C_7H_6O_2$ crystals stored in the PEG-DA beacons in their solid form.

beacons in their solid forms (Fig. 5C, inset). The timescale for SI interaction is, therefore, set by the solubility of the solid crystal in water, rather than by the partition coefficient or association constant of the solute with the gel.

The reaction between $Ca(OH)_2$ and $C_7H_6O_2$ obeys the following stoichiometry

$$2C_7H_5O_2^- + 2H^+ + Ca^{2+} + 2OH^- \rightleftharpoons 2H_2O + Ca(C_7H_5O_2)_2 \quad (1)$$

implying that H^+ and OH^- fluxes abruptly terminate at the reaction zone, where they react to form water. It was recently shown that solute reactions (acid-base) may cause colloids to focus diffusiophoretically (*34*). This is observed at the reaction between $Ca(OH)_2$ and $C_7H_6O_2$, where positive PS particles focus (Fig. 6A) and negative PS particles defocus (Fig. 6B). While focusing is directly evident in the micrographs, defocusing is more difficult to discern. In both cases, the velocity on the right-hand side of the reaction zone is greater than that on the left, causing a defocusing when particles move from left to right (negative PS) and a focusing when they move from right to left (positive PS). In addition, the reaction zone ($\tilde{x}_R$) gradually shifts toward the acidic beacon, which is a consequence of the ratio of diffusivities and solubilities of the two reactive species in water and the reaction stoichiometry (see the Supplementary Materials, fig. S3).

DISCUSSION

We have shown here that beacons can be triggered externally to release trapped solutes and consequently initiate SI interactions by simply changing the local temperature in the beacon. We acknowledge that this is only one class of stimuli-responsive beacon materials, and users of such interactions might further expand on this work by designing beacons that can be activated by complimentary triggers such as light (*39*, *40*), pH (*41*), electric field (*42*), or ultrasound (*43*), drawing inspiration from the controlled drug delivery literature (*44*).

Using different combinations of two or more beacons, we have also demonstrated distinct strategies to direct and enhance colloidal migration over distances that are hundreds of times further than typical equilibrium suspension interactions. Each of our different strategies comes with unique benefits, and one might be preferred depending on the specific application. The source-sink dipole system requires minimal raw material input (only one solute is needed) and is a clean system as solute is absorbed by the sink. Moreover, the system is conceptually straightforward and simple mass transport models capture the experimental nuances, allowing theoretical prediction of behavior.

Any combination of solutes can be used in the multisource system, which gives freedom to tailor the directionality and speed of migration. Each solute-particle interaction adds a degree of control. This suggests the use of multiple beacons and solutes to separate multicomponent suspensions and enable beacon-specific targeted delivery. The multisource system with reactive solutes adds a further degree of tunability by introducing the ability to focus or defocus particles at intermediate locations. The chemical reaction maintains low background concentrations, maintaining larger velocities for longer durations. Solute outflux in the distinct multibeacon strategies discussed here is mass transport limited; however, these beacons could, in principle, be replaced by pNIPAm beacons to initiate interactions on demand.

Any solute gradient can potentially induce colloidal motion, so long as the solute interacts with the particle surface. The interaction may be electrostatic in nature, in which case the particles migrate via DP. It may

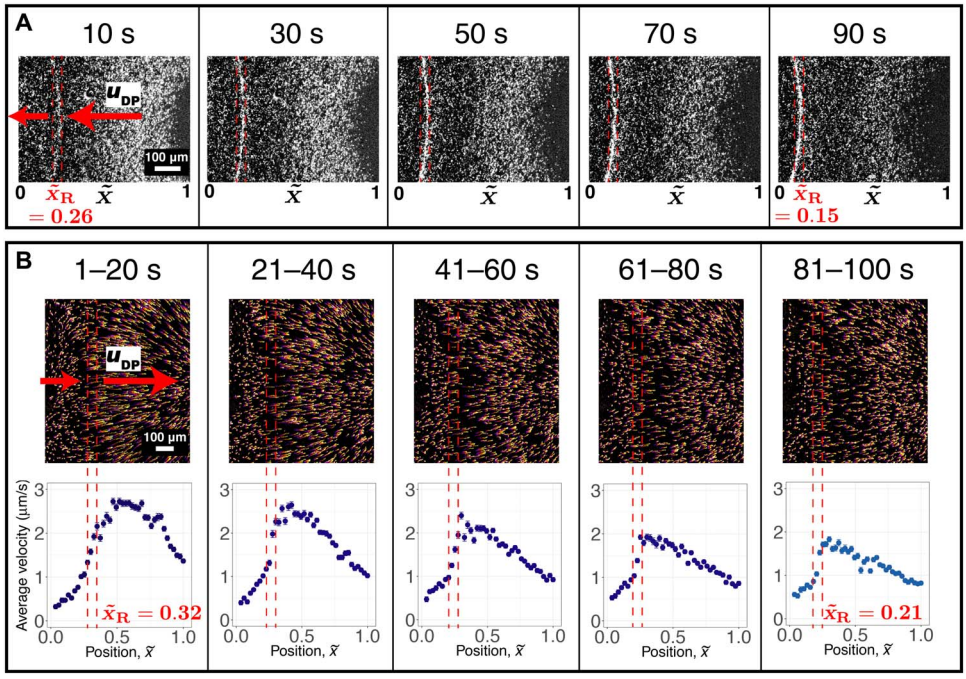

Fig. 6. Focusing and defocusing of particles migrating under an acid-base flux. (**A**) Positive PS particles focus at the reaction zone. (**B**) Negative PS particles defocus at the reaction zone, which is defined as the region where a maximum change in velocity is observed. The reaction zone ($\tilde{x}_R$) gradually shifts to the left (toward the acid source) over the course of the experiment. Error bars represent SD in average velocities over the time intervals. Positions are normalized by the distance between the two beacons.

also be driven by capillary/interfacial forces, where the solute reduces the surface tension of the particle, creating Marangoni stresses along the surface (*45*, *46*). These surface tension gradients cause the decane drops in Fig. 4 (C and D) to move toward higher concentrations of SDS, i.e., toward regions where the droplets can lower their surface tension in water. Chemical gradients may further give rise to density gradients, which could lead to density-driven fluid flows (*47*). Solute concentrations in our experiments, however, are small enough, and microfluidic geometries are confined enough that we neither expect nor observe buoyancy-driven convective flows. An interesting aspect to note is that PS particles in Figs. 3B and 4 (A and D, inset) accumulate at the back of the beacon absorbing SDS. We hypothesize that this is due to the formation of a concentration gradient around the periphery, pertaining to slow intradiffusion of SDS within the beacon.

The difficulty in modeling systems with more than one interacting solute species stems from the fact that concentration profiles in these systems are not simply additive. In multicomponent electrolyte systems, the ionic fluxes balance one another to maintain local electroneutrality, resulting in a net electric field that drives the DP migration. Thus, detailed information on the specific ion concentration profiles between the sources is required to use classic DP theories and correctly predict resultant particle velocities (*48*). The nontrivial consequences of coupled, multicomponent fluxes are highlighted in the fact that the contribution of different sources do not superimpose in Fig. 4B and that the velocity profiles on either side of the reaction zone are discontinuous in Fig. 6, resulting in focusing or defocusing of particles in reactive systems.

We envision that suitably designed, controlled SI interactions will find a range of applications in soft matter and mesoscale systems. Researchers are starting to realize the ubiquity of the DP phenomenon (*49*) and have demonstrated its versatility in a variety of applications such as deposition of latex on steel (*20*), water purification (*25*), transport into and out of dead-end pores (*27*, *28*), self-propelling particles (*50*), and active matter (*51*, *52*). The strategies demonstrated here show that concentration gradients can be exploited as a controllable external field for suspension manipulation and may augment existing techniques for colloidal handling and processing. These may include sorting particles with similar size but different surface chemistry, driving particles to target regions and delivering active ingredients, enhancing rates of suspension flocculation in dilute suspensions where even commercial flocculants would take much longer to form aggregates, analyzing colloidal mixtures and phase behavior, directing colloidal assembly, and synthesizing novel materials.

MATERIALS AND METHODS

Device fabrication

A computer-controlled laser cutter (Trotec Speedy 100) cut the channel design into 60-μm-thick Scotch tape. This was stuck to a Petri dish, which was used as a master for making a polydimethylsiloxane (PDMS) replica of the design. The PDMS master was used to fabricate the device in "microfluidic stickers" [Norland Optical Adhesive 81 (NOA81); Norland Adhesive] (*53*). A glass cover slide was used to seal the device, with holes drilled to provide access for inlet and outlet tubing. A PDMS inlet was ozone bonded to the cover slide to provide support for pins and tubings. The device was then baked at 80°C for at least 4 hours to strengthen the bonding. For the triggered release experiments, the microfluidic device had same dimensions as the one used in our previous work (*30*). For the multibeacon experiments, a two-inlet, single-outlet microfluidic device was used, where the two inlets enabled the simultaneous flow of two different liquid streams side by side. The two inlets were 500 μm wide, while the center channel where the inlets merge had a width of 4000 μm.

Sample preparation

Precursor solutions of pNIPAm were prepared by mixing 1 M NIPAM (Sigma-Aldrich) solution with 0.5 mol % cross-linker (*N*,*N*-methylenebisacrylamide; Sigma-Aldrich) and 5 mol % photoinitiator (α-ketoglutaric acid; Sigma-Aldrich) in deionized (DI) water; polyethylene glycol diacrylate (PEG-DA) precursor solutions were prepared by mixing 33% (v/v) PEG(700)-DA (Sigma-Aldrich) with 4% (v/v) photoinitiator (2-hydroxy-2-methylpropiophenone; Sigma-Aldrich) in DI water. Stock solutions of SDS (Sigma-Aldrich), [C_6mim][I] (Sigma-Aldrich), and NaOH (EMD Millipore) in DI water, and $CaCl_2.2H_2O$ (Sigma-Aldrich) and benzoic acid (Acros Organics) in ethanol were prepared and diluted according to the experimental requirements; negative and positive PS suspensions were prepared by suspending 0.25% (v/v) fluorescent sulfonated PS beads, 1 μm in diameter (FS03F; Bangs Laboratories), and 0.5% (v/v) aminated PS beads, 1.8 μm in diameter (PA04N; Bangs Laboratories), respectively, in DI water. Surfactant-free suspensions of decane drops were created by sonicating 2% (v/v) decane (Sigma-Aldrich) in DI water for 1 min.

Experimental setup

Hydrogel (beacon)

pNIPAm and PEG-DA gels were used as SI structures and fabricated using the microscope projection lithography technique (*54*). An ultraviolet (UV) lamp was set to 30 mW/cm^2 (measured at an empty objective slot). A 1000-μm diameter circular photomask was inserted into the field stop of an inverted microscope (Nikon TE-2000U) and aligned as described previously (*55*). pNIPAm/PEG-DA precursor solution was injected until the channel was filled. The syringe was disconnected, and 2 min was allowed for flow to relax. Then, 20-s (for pNIPAm gels) and 500-ms (for PEG-DA gels) UV exposures were used with a 10× objective to photopolymerize the gel. This step results in hydrogel posts with diameters 375 to 425 μm. The precursor solution was flushed from the device by flowing DI water for 2 hours for the PEG-DA gels. An NOA81 post was used as the inert structure in Fig. 3C and fabricated using the same procedure as with the PEG-DA beacons.

The pNIPAm gel was flushed with DI water for 24 hours for the control experiment, and only 10 min when some amount of residual photoinitiator was desired inside the gel. The microfluidic device was mounted on a thermal stage (Instec TSA12Gi) to control the temperature of the pNIPAm gel. The device was maintained at 50°C at the beginning of the experiment. Negative PS suspension at the same temperature was introduced into the device, flow was stopped using technique described in (*35*), and video recording (Andor iXon 885 fluorescence camera) was started with a 4× objective at one frame per second with 0.1 s exposure time. The temperature of the stage was then lowered to 25°C to allow the gel to cool down and cross the LCST. Video recording was stopped 30 min after the gel undergoes the transition.

Source-sink dipole

Two streams, one with 5 mM SDS in water and the other with clean DI water, were flowed simultaneously into the channel using the two inlets of the device. In this way, one of the beacons (the source) was loaded with SDS, while the other (sink) remained unloaded. After loading the source for 20 min, the two streams were flushed out by displacing with the suspension of negative PS particles. The flow was stopped, and video recording was started.

Multiple sources

Two streams, one with 5 mM SDS in water and the other with 5 mM [C_6mim][I] in water, were flowed simultaneously into the channel. Both the sources were loaded for 20 min before flushing with a suspension of negative PS particles/decane drops. Flow was stopped, and image series were recorded.

Multiple sources with reaction

Two streams, one with $CaCl_2.2H_2O$ (0.15 g/ml) in ethanol and the other with benzoic acid (0.4 g/ml) in ethanol, were flowed simultaneously into the channel. The two beacons were loaded for 10 min and subsequently flushed with NaOH (0.08 g/ml) in water and DI water, respectively. The NaOH reacts with $CaCl_2$ to precipitate out $Ca(OH)_2$ in the first beacon, while water reduces solvent quality for benzoic acid, resulting in benzoic acid crystal formation in the second beacon (Fig. 5C, inset). The two streams were then flushed by displacing with the PS suspensions. Flow was stopped, and image series were recorded.

Data analysis

Particles were identified and trajectories were linked from the fluorescence micrographs following the same procedure, as described previously (*30*). The azimuthal velocity in Fig. 3D was calculated by first dividing the micrograph along the line of symmetry ($y = 0$) and analyzing only one half (to reduce computation time). Instantaneous particle velocities in the radial and tangential directions were obtained from frame-to-frame displacements, and velocity profiles were calculated by averaging the velocities within angular regions of 5° width with the origin fixed at the center of the source. The velocity profiles were further averaged over an interval of 500 s. The space average velocities in Figs. 4C and 5C were extracted by first cropping the micrograph in the space between the two beacons into rectangular regions with approximate dimensions, 320 by 250 pixels, and then measuring the displacement of the particles in the x direction (and, hence, the x component of the velocity). The velocity profiles were calculated independently over 10-s intervals throughout the experiment, and averaged over all of space. Velocity for single-source systems in these cases refers to the average velocity of particles in the space between source-sink beacon pairs of corresponding solutes. The time average velocities in Fig. 6B were also extracted in the same way as the space average velocities. The velocity profiles in this case were, however, calculated by averaging the velocities within spatial bins of 10-pixel width and further averaged over the given time interval. Splitting the experiment into chunks in this way provides more samples in each bin, improving the statistics of averaging and suppressing noise in the velocity profiles. The particle flux in Fig. 3 (E and F) was calculated by directly counting the number of particles entering and exiting a region of radius $r \approx 300\ \mu m \approx 1.5{*}R_{beacon}$ around the sink. This number was then normalized by the total number of particles counted in that region at the beginning of the experiment. The particle flux for a single source (blue points in Fig. 3, E and F) was calculated by counting the number of particles entering an imaginary ring (of $r \approx 300\ \mu m$), situated at the same location as the sink in the source-sink experiments.

COMSOL model for SI dipole

The *Transport of Diluted Species* module of COMSOL Multiphysics was used to numerically solve the coupled solute and particle conservation equations (details in the Supplementary Materials). The microfluidic device and beacon dimensions used for the computations were directly obtained from experimental measurements, and other physical parameters such as the diffusion coefficient of SDS were obtained from the literature. Space was meshed with a triangular mesh, and solute and particle concentration profiles were calculated. Results were then exported in matrix form and postprocessed in R to obtain radial (V_r) and azimuthal (V_ϕ) particle velocities.

SUPPLEMENTARY MATERIALS

Supplementary material for this article is available at http://advances.sciencemag.org/cgi/content/full/5/8/eaax1893/DC1

Fig. S1. Colloidal migration under α-ketoglutaric acid gradients.
Fig. S2. Negatively charged PS particles move down α-ketoglutaric acid gradients.
Fig. S3. DP focusing/defocusing under acid-base gradients.
Table S1. Parameters used for numerically calculating the concentration profile of PS particles migrating under an SDS flux, generated by a source-sink pair of SI beacons.
Table S2. Diffusivity and solubility of benzoic acid and calcium hydroxide in water.
Movie S1. A pNIPAm beacon with residual photoinitiator (α-ketoglutaric acid) undergoing phase transition at the LCST (33°C).
Movie S2. A pNIPAm beacon from which all the solute has been flushed out, undergoing phase transition at the LCST.
Movie S3. SI dipole interaction between a beacon source (left) that releases SDS and a beacon sink (right) that absorbs the solute.
Movie S4. COMSOL computations revealing the behavior of particles under an SI dipolar flux, reproducing the experimental observations of movie S3.
Movie S5. SI interaction between two sources releasing distinct solutes.
Movie S6. A beacon source releasing SDS attracts decane drops (black) and simultaneously repels negative PS particles (white).
Movie S7. Two distinct beacon sources, one releasing SDS (left) while the other releasing [C_6mim][I] (right), attract decane drops (black) and negative PS beads (white), respectively, separating them from the mixture.
Movie S8. SI migration of positively charged particles driven by beacon sources that release solutes that react with each other.
Movie S9. SI migration of negatively charged particles driven by beacon sources that release solutes that react with each other.

REFERENCES AND NOTES

1. V. N. Bakunin, A. Y. Suslov, G. N. Kuzmina, O. P. Parenago, A. V. Topchiev, Synthesis and application of inorganic nanoparticles as lubricant components—A review. *J. Nanopart. Res.* **6**, 273–284 (2004).
2. L. Goehring, J. Li, P.-C. Kiatkirakajorn, Drying paint: From micro-scale dynamics to mechanical instabilities. *Phil. Trans. R. Soc. A* **375**, 20160161 (2017).
3. G. Maitland, Transforming 'formulation': Systematic soft materials design. *Soft Matter* **1**, 93–94 (2005).
4. S. Q. Choi, S. Steltenkamp, J. A. Zasadzinski, T. M. Squires, Active microrheology and simultaneous visualization of sheared phospholipid monolayers. *Nat. Commun.* **2**, 312 (2011).
5. H.-X. Zhou, G. Rivas, A. P. Minton, Macromolecular crowding and confinement: Biochemical, biophysical, and potential physiological consequences. *Annu. Rev. Biophys.* **37**, 375–397 (2008).
6. B. Ruzicka, E. Zaccarelli, A fresh look at the Laponite phase diagram. *Soft Matter* **7**, 1268–1286 (2011).
7. P. L. Saldanha, V. Lesnyak, L. Manna, Large scale syntheses of colloidal nanomaterials. *Nano Today* **12**, 46–63 (2017).
8. E. Dickinson, Colloids in food: Ingredients, structure, and stability. *Annu. Rev. Food Sci. Technol.* **6**, 211–233 (2015).
9. C. Majidi, Soft Robotics: A perspective—Current trends and prospects for the future. *Soft Robot.* **1**, 5–11 (2014).
10. R. L. Truby, J. A. Lewis, Printing soft matter in three dimensions. *Nature* **540**, 371–378 (2016).
11. H. Löwen, Colloidal soft matter under external control. *J. Phys. Condens. Matter* **13**, R415–R432 (2001).
12. J. N. Israelachvili, *Intermolecular and Surface Forces* (Academic Press, ed 3, 2011).
13. H. Löwen, Colloidal dispersions in external fields. *J. Phys. Condens. Matter* **24**, 460201 (2012).
14. J. Palacci, S. Sacanna, A. P. Steinberg, D. J. Pine, P. M. Chaikin, Living crystals of light-activated colloidal surfers. *Science* **339**, 936–940 (2013).
15. J. J. Juárez, P. P. Mathai, J. A. Liddle, M. A. Bevan, Multiple electrokinetic actuators for feedback control of colloidal crystal size. *Lab Chip* **12**, 4063–4070 (2012).
16. P. Dillmann, G. Maret, P. Keim, Two-dimensional colloidal systems in time-dependent magnetic fields. *Eur. Phys. J. Spec. Top.* **222**, 2941–2959 (2013).

17. C. Eisenmann, C. Kim, J. Mattsson, D. A. Weitz, Shear melting of a colloidal glass. *Phys. Rev. Lett.* **104**, 035502 (2010).
18. H. Löwen, Twenty years of confined colloids: from confinement-induced freezing to giant breathing. *J. Phys. Condens. Matter* **21**, 474203 (2009).
19. M. Cavallaro Jr., L. Botto, E. P. Lewandowski, M. Wang, K. J. Stebe, Curvature-driven capillary migration and assembly of rod-like particles. *Proc. Natl. Acad. Sci. U.S.A.* **108**, 20923–20928 (2011).
20. B. V. Derjaguin, S. S. Dukhin, A. A. Korotkova, Diffusiophoresis in electrolyte solutions and its role in the Mechanism of the formation of films from caoutchouc latexes by the ionic deposition method. *Prog. Surf. Sci.* **43**, 153–158 (1993).
21. D. C. Prieve, Migration of a colloidal particle in a gradient of electrolyte concentration. *Adv. Colloid Interf. Sci.* **16**, 321–335 (1982).
22. D. C. Prieve, J. L. Anderson, J. P. Ebel, M. E. Lowell, Motion of a particle generated by chemical gradients. Part 2. Electrolytes. *J. Fluid Mech.* **148**, 247–269 (1984).
23. J. L. Anderson, Colloid transport by interfacial forces. *Annu. Rev. Fluid Mech.* **21**, 61–99 (1989).
24. J. J. McDermott, A. Kar, M. Daher, S. Klara, G. Wang, A. Sen, D. Velegol, Self-generated diffusioosmotic flows from calcium carbonate micropumps. *Langmuir* **28**, 15491–15497 (2012).
25. S. Shin, O. Shardt, P. B. Warren, H. A. Stone, Membraneless water filtration using CO 2. *Nat. Commun.* **8**, 15181 (2017).
26. D. Florea, S. Musa, J. M. R. Huyghe, H. M. Wyss, Long-range repulsion of colloids driven by ion exchange and diffusiophoresis. *Proc. Natl. Acad. Sci. U.S.A.* **111**, 6554–6559 (2014).
27. A. Kar, T.-Y. Chiang, I. Ortiz Rivera, A. Sen, D. Velegol, Enhanced transport into and out of dead-end pores. *ACS Nano* **9**, 746–753 (2015).
28. S. Shin, E. Um, B. Sabass, J. T. Ault, M. Rahimi, P. B. Warren, H. A. Stone, Size-dependent control of colloid transport via solute gradients in dead-end channels. *Proc. Natl. Acad. Sci.* **113**, 257–261 (2016).
29. A. Kar, R. Guha, N. Dani, D. Velegol, M. Kumar, Particle deposition on microporous membranes can be enhanced or reduced by salt gradients. *Langmuir* **30**, 793–799 (2014).
30. A. Banerjee, I. Williams, R. N. Azevedo, M. E. Helgeson, T. M. Squires, Soluto-inertial phenomena: Designing long-range, long-lasting, surface-specific interactions in suspensions. *Proc. Natl. Acad. Sci. U.S.A.* **113**, 8612–8617 (2016).
31. J. C. Berg, *An Introduction to Interfaces & Colloids: The Bridge to Nanoscience* (World Scientific, 2010).
32. R. H. Pelton, P. Chibante, Preparation of aqueous latices with *N*-isopropylacrylamide. *Colloids Surf.* **20**, 247–256 (1986).
33. Y. Hirokawa, T. Tanaka, Volume phase transition in a nonionic gel. *J. Chem. Phys.* **81**, 6379–6380 (1984).
34. N. Shi, R. Nery-Azevedo, A. I. Abdel-Fattah, T. M. Squires, Diffusiophoretic Focusing of Suspended Colloids. *Phys. Rev. Lett.* **117**, 258001 (2016).
35. J. S. Paustian, C. D. Angulo, R. Nery-Azevedo, N. Shi, A. I. Abdel-Fattah, T. M. Squires, Direct measurements of colloidal solvophoresis under imposed solvent and solute gradients. *Langmuir* **31**, 4402–4410 (2015).
36. R. Nery-Azevedo, A. Banerjee, T. M. Squires, Diffusiophoresis in Ionic Surfactant Gradients. *Langmuir* **33**, 9694–9702 (2017).
37. K. C. Tam, E. Wyn-Jones, Insights on polymer surfactant complex structures during the binding of surfactants to polymers as measured by equilibrium and structural techniques. *Chem. Soc. Rev.* **35**, 693–709 (2006).
38. S. Luo, S. Zhang, Y. Wang, A. Xia, G. Zhang, X. Du, D. Xu, Complexes of ionic liquids with poly(ethylene glycol)s. *J. Organomet. Chem.* **75**, 1888–1891 (2010).
39. A. M. Kloxin, A. M. Kasko, C. N. Salinas, K. S. Anseth, Photodegradable hydrogels for dynamic tuning of physical and chemical properties. *Science* **324**, 59–63 (2009).
40. S. Helmy, F. A. Leibfarth, S. Oh, J. E. Poelma, C. J. Hawker, J. R. de Alaniz, Photoswitching using visible light: A new class of organic photochromic molecules. *J. Am. Chem. Soc.* **136**, 8169–8172 (2014).
41. S. Zhang, A. M. Bellinger, D. L. Glettig, R. Barman, Y.-L. Lee, J. Zhu, C. Cleveland, V. A. Montgomery, L. Gu, L. D. Nash, D. J. Maitland, R. Langer, G. Traverso, A pH-responsive supramolecular polymer gel as an enteric elastomer for use in gastric devices. *Nat. Mater.* **14**, 1065–1071 (2015).
42. S. Murdan, Electro-responsive drug delivery from hydrogels. *J. Control. Release* **92**, 1–17 (2003).
43. N. Huebsch, C. J. Kearney, X. Zhao, J. Kim, C. A. Cezar, Z. Suo, D. J. Mooney, Ultrasound-triggered disruption and self-healing of reversibly cross-linked hydrogels for drug delivery and enhanced chemotherapy. *Proc. Natl. Acad. Sci. U.S.A.* **111**, 9762–9767 (2014).
44. J. Li, D. J. Mooney, Designing hydrogels for controlled drug delivery. *Nat. Rev. Mater.* **1**, 1607 (2016).
45. B. G. Levich, A. M. Kuznetsov, On the motion of drops in liquids under the action of surface active substances. *Dokl. Akad. Nauk SSSR* **146**, 145–147 (1962).
46. T. M. Squires, S. R. Quake, Microfluidics: Fluid physics at the nanoliter scale. *Rev. Mod. Phys.* **77**, 977–1026 (2005).
47. S. Das, O. E. Shklyaev, A. Altemose, H. Shum, I. Ortiz-Rivera, L. Valdez, T. E. Mallouk, A. C. Balazs, A. Sen, Harnessing catalytic pumps for directional delivery of microparticles in microchambers. *Nat. Commun.* **8**, 14384 (2017).
48. T.-Y. Chiang, D. Velegol, Multi-ion diffusiophoresis. *J. Colloid Interface Sci.* **424**, 120–123 (2014).
49. D. Velegol, A. Garg, R. Guha, A. Kar, M. Kumar, Origins of concentration gradients for diffusiophoresis. *Soft Matter* **12**, 4686–4703 (2016).
50. J. F. Brady, Particle motion driven by solute gradients with application to autonomous motion: Continuum and colloidal perspectives. *J. Fluid Mech.* **667**, 216–259 (2011).
51. I. Theurkauff, C. Cottin-Bizonne, J. Palacci, C. Ybert, L. Bocquet, Dynamic clustering in active colloidal suspensions with chemical signaling. *Phys. Rev. Lett.* **108**, 268303 (2012).
52. A. C. Balazs, P. Fischer, A. Sen, Intelligent nano/micromotors: Using free energy to fabricate organized systems driven far from equilibrium. *Acc. Chem. Res.* **51**, 2979 (2018).
53. D. Bartolo, G. Degré, P. Nghe, V. Studer, Microfluidic stickers. *Lab Chip* **8**, 274–279 (2008).
54. D. Dendukuri, S. S. Gu, D. C. Pregibon, T. A. Hatton, P. S. Doyle, Stop-flow lithography in a microfluidic device. *Lab Chip* **7**, 818–828 (2007).
55. J. S. Paustian, R. N. Azevedo, S. T. B. Lundin, M. J. Gilkey, T. M. Squires, Microfluidic microdialysis: Spatiotemporal control over solution microenvironments using integrated hydrogel membrane microwindows. *Phys. Rev. X* **3**, 041010 (2013).

Acknowledgments: We thank J. Eriksson, I. Williams, N. Shi, A. Bayles, and J. Read de Alaniz for the valuable discussions. A portion of this work was performed in the Microfluidics Laboratory and the Biological Nanostructures Laboratory within the California NanoSystems Institute, supported by the University of California, Santa Barbara (UCSB), and the University of California, Office of the President, and in the Shared Experimental Facilities of the Materials Research Science and Engineering Center at UCSB (MRSEC NSF DMR 1720256). **Funding:** We gratefully acknowledge support from the National Science Foundation (NSF) under grant CBET-1438779 and the Saudi Arabian Oil Company (Saudi Aramco Contract A-0002-2018). **Competing interests:** The authors declare that they have no competing interests. **Author contributions:** A.B. and T.M.S. conceived the project. A.B. performed the experiments and analyzed the data. A.B. and T.M.S. discussed the results and wrote the paper. **Data and materials availability:** All data needed to evaluate the conclusions in the paper are present in the paper and/or the Supplementary Materials. Additional data related to this paper may be requested from the authors.

Submitted 28 February 2019
Accepted 10 July 2019
Published 16 August 2019
10.1126/sciadv.aax1893

Citation: A. Banerjee, T. M. Squires, Long-range, selective, on-demand suspension interactions: Combining and triggering soluto-inertial beacons. *Sci. Adv.* **5**, eaax1893 (2019).